SCIENTIFIC SUMMARIES

Anomalies of the Electronic Structure and Physical Properties of Rare-Earth Cobaltites near Spin Crossover[1]

V. A. Dudnikov[a], Yu. S. Orlov[a, b, *], N. V. Kazak[a], M. S. Platunov[a], and S. G. Ovchinnikov[a]

[a] *Kirensky Institute of Physics, Siberian Branch, Russian Academy of Sciences, Krasnoyarsk, 660036 Russia*
[b] *Siberian Federal University, Krasnoyarsk, 660041 Russia*
* e-mail: jso.krasn@mail.ru
Received August 25, 2016; in final form, September 15, 2016

The features of the characteristics of $LnCoO_3$ cobaltites, where Ln is a rare-earth element, are discussed. Both experiment and theory demonstrate that their essentials are related to the low-spin ground state of cobalt ions. The thermally induced occupation of the excited high-spin state gives rise to peaks in the magnetic susceptibility, specific heat, and thermal expansion, as well as to a smooth insulator—metal transition. The analysis is based both on the data from the current literature concerning $LaCoO_3$ and in many aspects on our own studies of $GdCoO_3$ and $La_{1-x}Gd_xCoO_3$ solid solutions.

1. INTRODUCTION

Similarly to other perovskite oxides such as cuprates and manganites, rare-earth cobaltites belong to strongly correlated electron systems. At the same time, they exhibit a unique feature: the filling of the d^6 shell of the Co^{3+} ion does not obey Hund's rule, and the ground state is the low-spin (LS) atomic term with $S = 0$ instead of the high-spin (HS) state with spin $S = Z$. Hund's rule is violated because the crystal field $10Dq$ (which lowers the energy of the LS term) exceeds the critical value determined by the competition with Hund's coupling constant J. As a result, spin crossover occurs: the levels corresponding to the HS term E_{HS} and those of the LS term E_{LS} intersect at some point with the growth in the $10Dq/J$ ratio. This phenomenon was discovered rather long ago [1]. It is clearly seen in the Tanabe—Sugano diagrams for d^4, d^5, d^6, and d^7 ions [2]. Currently, two classes of materials with spin crossovers are of common knowledge. The first one includes organometallic compounds with magnetic ions [3]. In such compounds, the crossover is achieved by changing the temperature of a compound or by applying a relatively low pressure. Another class is formed by the Mott—Hubbard insulators, mainly iron oxides, with predominantly ionic chemical bonds. They exhibit the crossover at high pressures, $P \sim 100$ GPa [4].

Rare-earth cobaltites belong to the second group of compounds, but in contrast to iron oxides, they turn out to be in the LS state already at $T = 0$ and at zero applied pressure; i.e., the spin crossover already occurs in the course of the formation of their structure owing to the "chemical pressure" determining the equilibrium volume of the unit cell. The vicinity to the spin crossover is characterized by the spin gap $\Delta_S = E_{HS} - E_{LS}$. In iron oxides, where $\Delta_S < 0$ and $|\Delta_S| \sim 1$ eV at zero applied pressure, even a slight change in temperature affects the spin crossover, whereas the corresponding value in $LaCoO_3$ is $\Delta_S \sim 0.01$ eV. If La is replaced by heavier rare-earth ions, the spin gap increases [5] owing to the lanthanide compression; nevertheless, the typical value is $\Delta_S \sim 0.1$ eV. Just this small energy scale in rare-earth cobaltites underlies their specific electron, magnetic, and thermal characteristics, which will be considered in the present review article. The further plan of the paper is the following. In Section 2, we present the main experimental facts from the available publications and from our own studies on underdoped stoichiometric $LnCoO_3$ cobaltite and on the compounds with isovalent substitution. In Section 3, we discuss the multielectron nature of the formation of electron and magnetic properties near the spin crossover. Section 4 deals with the specific features of cobaltites with heterovalent substitution. The final remarks are presented in Section 5.

2. PROPERTIES OF UNDERDOPED COBALTITES

Similarly to the other transition metals (iron, copper, or manganese), cobalt can exhibit several possible

---

[1] Supplementary material is available at http://link.springer.com/.

valence states (Co^{2+}, Co^{3+}, and Co^{4+}) and can have different coordination geometry, namely, tetrahedral, octahedral, and pyramidal. As a result, structures with mixed cobalt valence and nonstoichiometric compounds with oxygen vacancies can exist. Hund's rule implies that Co^{2+} is always in the high-spin state $t_{2g}^5 e_g^2$ ($S = 3/2$), whereas Co^{4+} is usually in the low-spin state, $t_{2g}^5 e_g^0$ ($S = 1/2$). The possible states of Co^{3+}—low-spin $t_{2g}^6 e_g^0$ (LS, $S = 0$), high-spin $t_{2g}^4 e_g^2$ (HS, $S = 2$), and intermediate-spin $t_{2g}^5 e_g^1$ (IS, $S = 1$) (see Fig. 1 in the supplementary material)—appear to be very sensitive to the magnitude of the crystal field, i.e., to the changes in the Co—O bond lengths and in the Co—O—Co angles [6]. Some unique properties both of underdoped stoichiometric perovskite-type oxides and of the compounds with isovalent and heterovalent substitution of the rare earth are described in many review articles (see, e.g., [7, 8]).

The active study of rare-earth cobaltites was initiated by the anomalous behavior of the temperature dependence of the magnetic susceptibility in $LaCoO_3$, which exhibits two smeared peaks near $T_1 \approx 150$ K and $T_2 \approx 500$ K (see the lower panel of Fig. 2 in the supplementary material) [9–12]. In the first attempts at explaining these magnetic anomalies, they were related both to the formation of a magnetic superstructure because of changes in the spin state of Co^{3+} ions [13–15] resulting from the close values of interatomic Hund's rule exchange energy J and the crystal-field energy $10Dq$ at Co^{3+} sites and to the assumption that the state with spin $S = 2$ becomes more favorable in energy than the low-spin state at a certain temperature. The low-temperature anomaly was associated with the spin-state transition of a certain part of Co^{3+} ions from the nonmagnetic $t_{2g}^6 e_g^0$ LS state to the paramagnetic $t_{2g}^4 e_g^2$ HS state, whereas a smeared peak in the temperature dependence of the magnetic susceptibility should correspond to the 1 : 1 ratio of the numbers of HS and LS ions [16]. The high-temperature anomaly was associated with a semiconductor–metal transition (see the upper panel of Fig. 2 in the supplementary material) and was interpreted as a consequence of the destruction of the spin-ordered state driven by the increase in mobility of e_g electrons accompanied by the transition of the remaining LS cobalt ions to the HS state. However, the further numerous experiments revealed neither any magnetic superstructure nor the long-range magnetic order in $LaCoO_3$. While the ground state of cobalt ions has without doubt been identified as the nonmagnetic LS state, the nature of the first excited state (IS or HS) has been under debate for many years. The possibility of the intermediate-spin state is supported by the

attempts to fit the $\chi(T)$ curve in $LaCoO_3$ at $T > 100$ K by the Curie law with the resulting value of spin S being nearer to unity than to two. The suggested two-stage model [17, 18] assuming that the first anomaly is related to the transition of cobalt from the LS to IS state, whereas the second one should be attributed to the IS—HS transition, which has been supported by the corresponding calculations [19–21], would seem to explain the existing controversy.

However, the calculations [19] in the framework of the LDA+U approach can be valid only for the hypothetical ferromagnetic phase, which does not actually exist. Therefore, it is unreasonable to enlist them to interpret the properties of $LaCoO_3$ and such interpretation can only mislead an inexperienced reader. Moreover, a series of ESR experiments [22] and the X-ray spectroscopy data [23] for the $LaCoO_3$ compound, which appeared later on, suggested the transition of cobalt ions from low- to high-spin state. These data support the scheme of multielectron levels [24], in which the ground low-spin state is separated by the spin gap from the series of the high-spin terms with the total angular momentum $J = 1$, 2, and 3. According to the neutron scattering data, the cobaltites with Pr, Nd, Sm, and Eu do not exhibit any traces of the high-spin state up to room temperature [25].

The active studies of the magnetic, transport, and thermal properties of the other compounds in the $LnCoO_3$ series demonstrate that they exhibit the same features in the behavior of the magnetic susceptibility, thermal expansion (see Fig. 3 in the supplementary material), specific heat, and electrical conductivity (see Fig. 4 in the supplementary material) as those observed in $LaCoO_3$ [26–33]. At the same time, the anomalies in the behavior of $\chi(T)$, $\alpha(T)$, $C_P(T)$, and $\rho(T)$ become shifted toward higher temperatures and more smoothed, exhibiting the correlation between the transport and thermal properties. The obtained data allow drawing the electron phase diagram for the series of lanthanides demonstrating the dependence of the properties on the ionic radius r_R (see Fig. 5 in the supplementary material) [34]. In this diagram, we can outline three states: the nonmagnetic insulator, paramagnetic insulator, and paramagnetic metal. The smooth and smeared transitions between these states suggest that we are dealing with the crossovers rather than with the phase transitions in their classical meaning.

The structural studies of the rare-earth $LnCoO_3$ cobaltites [14, 35–38] have demonstrated that all stoichiometric $LnCoO_3$ oxides are not perfect $Pm3\bar{m}$-type cubic perovskites (see Fig. 6 in the supplementary material), and those with Ln ≠ La belong to the $Pbnm$ space group (see Fig. 7 in the supplementary material) or to the similar $Pbna$ group obtained by the rearrangement of the crystallographic axes. The magni-

tude of distortions changes depending on the specific choice of lanthanide. The smallest distortions are observed in the $NdCoO_3$ compound.

We focused our efforts on the studies of $LnCoO_3$ and $La_{1-x}Ln_xCoO_3$ compounds, choosing Gd^{3+} as the rare-earth element. Gadolinium was chosen because this ion has a constant valence and zero orbital angular momentum ($L = 0$, $S = 7/2$). Therefore, in the compounds under study, we do not need to take into account the contributions from the Pauli and Van Vleck paramagnetism. The effective magnetic moment per formula unit, $\mu_{eff} \approx 7.91\mu_B$, obtained in experiment for $GdCoO_3$ [39] nearly coincides in the low-temperature range with the theoretical value $\mu_{eff} \approx 7.94\mu_B$. This confirms the nonmagnetic state for Co^{3+} ions and agrees with the earlier results [40–43]. At the temperature $T_N = 3.3$ K, the gadolinium sublattice undergoes the transition to the antiferromagnetic state.

To determine the additional chemical pressure similar to the hydrostatic one and arising at the substitution of a rare-earth element by another rare-earth element with a smaller ionic radius, we use the Birch–Murnaghan equation of state [44, 45]

$$P = \frac{3}{2}B_0\left[\left(\frac{V_0}{V}\right)^{7/3} - \left(\frac{V_0}{V}\right)^{5/3}\right]$$
$$\times\left\{1 - \frac{3}{4}(4 - B_0')\left[\left(\frac{V_0}{V}\right)^{2/3} - 1\right]\right\},$$

where B_0 and B_0' are empirical parameters having the physical meaning of the isothermal bulk modulus and of its first pressure derivative, respectively ($B_0' = 4$ for the perovskite-type cobaltites and $B_0 = 150$ GPa for $LaCoO_3$ [6]); V_0 is the volume of the unit cell for $LaCoO_3$; and V is the volume of the unit cell for Ln lanthanide. Assuming also that the intraband parameters of the Coulomb interaction (Racah parameters) are the same for Co^{3+} in $LaCoO_3$ and $GdCoO_3$, we have managed to estimate the increase in the crystal field resulting from the "lanthanide" compression and the width of the spin gap in $GdCoO_3$ ($\Delta_S \approx 2000$ K) [46]. At the same time, taking the volumes of the unit cells from the current literature, we are able to estimate the spin gap width for the whole lanthanide series (see Fig. 8 in the supplementary material) [5, 46].

The X-ray diffraction and the temperature dependence of the dc magnetization for $GdCoO_3$ within the high-temperature range (from 298 to 1273 K) demonstrate [47], first, the pronounced asymmetric broadening of the diffraction peaks, which gradually decrease and disappear at higher and lower temperatures (see Fig. 9 in the supplementary material), and,

second, an additional growth with temperature contribution to the magnetic susceptibility provided by Co^{3+} ions (see Fig. 10 in the supplementary material).

The thorough study of the temperature dependence for the lattice parameters and ab initio calculations using the DFT–GGA technique allow us to formulate the model of virtual crystal [47, 48], where the domains with cobalt ions in the LS and HS states coexist in a certain temperature range (from 200 to 700 K for $GdCoO_3$). Using this model, we establish the relation between the anomalously high thermal expansion in $GdCoO_3$ and fluctuations of the multiplicity. We also obtain the expression for the molar magnetic susceptibility χ_{Co} of cobalt in the form of the Curie–Weiss law with the effective constant C_{eff} and the Curie temperature Θ_{eff} depending on the population n_{HS} of the high-spin state

$$\chi_{Co} = N_A\frac{C_{eff}}{3k_B(T - \Theta_{eff})},$$

$$C_{eff} = g^2\mu_B^2 S(S + 1)n_{HS},$$

$$n_{HS}(T) = \frac{g_{HS}\exp(-\Delta_S/k_BT)}{1 + g_{HS}\exp(-\Delta_S/k_BT)}.$$

The magnetic susceptibility of Co^{3+} ions calculated in such a way is illustrated in the inset of Fig. 10 in the supplementary material. On the basis of this model, we have calculated the temperature dependence of magnetic susceptibility of $La_{1-x}Gd_xCoO_3$ samples, which appears to be in good agreement with the experimental data. Then, we have calculated the dependence of the spin gap on the concentration of dopants for the solid solution with the isovalent substitution [48] and demonstrated the possibility of controlling magnetic characteristics by changing the spin gap. The calculations based on the modified crystal field theory also confirm that the contribution to the magnetic susceptibility comes just from the high-spin cobalt ions; these calculations demonstrate that the energy corresponding to the intermediate state of cobalt ions is much higher than that of the high-spin state [49].

In spite of the obtained interpretation of some amazing properties of stoichiometric $LnCoO_3$ rare-earth cobaltites, the studies of these materials do not stop. In particular, the studies of $LaCoO_3$ in ultrahigh magnetic fields up to 133 T at different temperatures reported in [50] reveal an unusual magnetic field dependence of the magnetization (see Fig. 11 in the supplementary material).

3. MULTIELECTRON NATURE OF THE FORMATION OF ELECTRON AND MAGNETIC PROPERTIES NEAR SPIN CROSSOVER

Perovskite-type cobalt oxides being close to the spin crossover exhibit fluctuations of the spin and orbital multiplicity of cobalt ions and this causes many peculiar features of the magnetic, electrical, and structural characteristics. The additional degrees of freedom related to the fluctuations of multiplicity affect also such transport characteristics as electrical and thermal conductivities, giving rise to unusually high thermoelectric coefficients in cobaltites.

In addition, many properties of the compounds under study are quite sensitive to different kinds of disorder and to the oxygen nonstoichiometry. For example, a slight deviation of the oxygen content from the stoichiometric one ($\delta < 0.002$) leads to the change in sign and in the temperature dependence of thermoelectric power in $LaCoO_{3-\delta}$. Another example is $GdCoO_3$, which is a semiconductor with the band gap $E_g \approx 0.5$ eV (according to the measurements of electrical transport characteristics). It has unusual optical absorption spectra without the transparency window expected for a semiconductor. Instead of it, we observed a narrow transmission peak (see Fig. 1) [51]. To reconcile the data on the electrical conductivity and optical absorption, we studied the effect of oxygen vacancies on the electronic structure of $GdCoO_{3-\delta}$.

Nonstoichiometric oxides, nitrides, carbides, sulfides, and other compounds in the solid phase form a large class of disordered solid systems, which are actively studied both experimentally and theoretically owing to their unique physical and chemical characteristics. Therefore, the implementation of the techniques for electronic structure calculations allowing the description of nonstoichiometric compounds with disordered positions of vacancies is of special interest in itself.

For rare-earth cobalt oxides, there is still no unambiguous theoretical description of the scenario for the temperature-dependent transition of cobalt ions from the nonmagnetic to magnetic state. Indeed, for the formulation of such a scenario, we need to take simultaneously into account both the Coulomb correlation and the hybridization between oxygen p orbitals and cobalt d orbitals and to perform a detailed analysis of the temperature evolution of the multiplet states of cobalt ions. A specific feature of the energy band structure of these systems is the existence of the mutual overlapping and smearing of the hybridized and correlated states. Such a situation creates difficulties for the modeling of electronic structure for this type of compounds. The key problem is the effect of Coulomb correlations on the magnetic, lattice, and spectral characteristics of the systems with the predominantly ionic bonding type but also with a suffi-
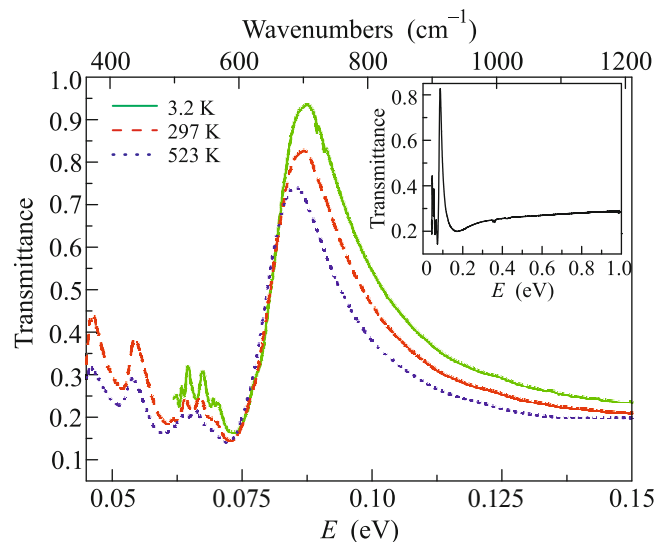

Fig. 1. (Color online) Transmission spectra of $GdCoO_{3-\delta}$ measured at temperatures $T =$ (solid line) 3.2, (dashed line) 297, and (dotted line) 523 K. The inset represents the spectrum obtained at room temperature within a broader energy range.

ciently strong covalent bonding related to the hybridization between the states of ligand and partially occupied states of metal. In the compounds under study, the correlation effects are important for the states near the Fermi level, which are described by hybridized wavefunctions.

Most of the methods used in condensed matter physics and in quantum chemistry for calculations of the electronic structure of solids are based on the density functional theory (DFT). The main problem of density functional theory is that exact analytical expressions for the functionals corresponding to the exchange and correlation energies are known only for the specific case of free electron gas. In the physical applications, the local density approximation (LDA) is the most popular one. This approximation assumes that the functional calculated at some point in space depends only on the electron density at this point.

The problem of strong electron correlations has been known for a long time, beginning from the seminal works by Mott and Hubbard. However, a satisfactory solution to this problem is still lacking. Such a situation occurs because the conventional perturbation theory is inapplicable for the systems with strong electron correlations, whereas the exact solution for the Hubbard model exists only for the one-dimensional case. A vivid example of the inapplicability of the standard methods of quantum theory based on the electron density functional theory is the erroneous metallic ground state for all perovskite-type cobalt oxides and of other underdoped Mott insulators. Therefore, the idea of developing some hybrid methods incorporating the power of the density functional approach

method with adequate involvement of strong electron correlations has been known for a long time. At present, we can emphasize two such approaches, namely, LDA + DMFT [52] and LDA + GTB [53, 54]. Both of these methods employ the wavefunction basis corresponding to the LDA. These basis functions are used for calculating the parameters of some simplified model Hamiltonian (usually of the Hubbard model in LDA + DMFT and of the multiband $p–d$ model in LDA + GTB). Both methods have their advantages and drawbacks, but in general, we can say that these two methods are complementary. The generalized tight-binding (GTB) method is constructed as a consistent cluster perturbation theory. In this approach, we can single out three stages.

(i) Dividing the infinite crystal lattice into a set of unit cells (clusters), e.g., CoO_6 clusters in the case of cobaltites. Since oxygen ions belong simultaneously to two neighboring cells, oxygen wavefunctions are orthogonalized and oxygen Wannier functions are constructed. The details of this procedure are described in [55]. Then, we perform the exact diagonalization of the intracell Hamiltonian and find the energies and multielectron wavefunctions corresponding to the local states; it is convenient to classify these states according to the number of electrons per cell.

(ii) Constructing the Hubbard X operators on the basis of local multielectron eigenstates. The calculation of matrix elements for electron creation operators on this basis allows us to write one-electron operators at a given site as a linear combination of Hubbard operators. After that, we perform a general perturbation theory analysis with the intersite hopping as a small parameter and formulate a generalized Dyson equation in the representation of Hubbard operators.

(iii) The multiband $p–d$ model with cation and anion orbitals involving the strong onsite Coulomb interaction at cations and the Coulomb interaction between cations and anions is exactly written in the form of the generalized Hubbard model including a set of local states and intercell hoppings, as well as interactions between them. Dispersion laws and the band structure of the fermion excitations appear owing to the intercell hoppings and are calculated using all the experience gained in the studies of strongly correlated electron systems in the Hubbard model in the limit of strong correlations. An important novelty of the theory under discussion is the dependence of the quasiparticle dispersion laws on the occupation numbers of the local states of different electron terms. In the present case, the temperature determines the occupancy of different multielectron terms and this leads to the clearly pronounced temperature dependence of the dispersion laws.

In Fig. 2, we compare the results of calculations of the band structure for the cubic $GdCoO_3$ crystal at $T = 0$ in the cases of (a) the LS ground state of cobalt
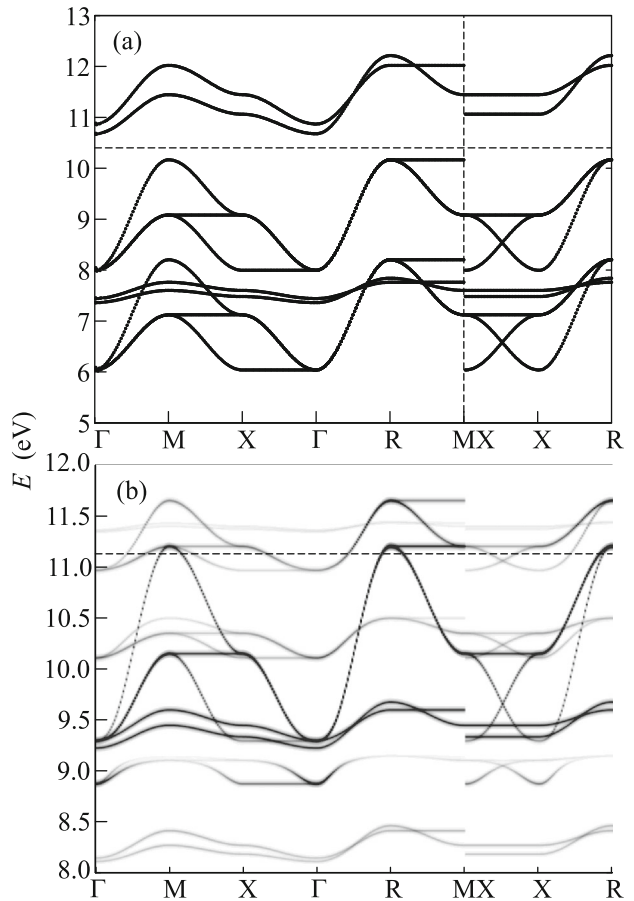

Fig. 2. Quasiparticle spectrum at $T = 0$ for (a) the LS phase and (b) the hypothetical HS phase (see the main text) of $GdCoO_3$ crystal. $G(0, 0, 0)$, $M(\pi, \pi, 0)$, $X(\pi, 0, 0)/(0, \pi, 0)$, and $R(\pi, \pi, \pi)$ are the symmetry points of the Brillouin zone. The dashed line shows the position of the chemical potential.

ions (LS phase) and (b) the artificially created HS state (this is a hypothetical HS phase, for which the HS ground state of cobalt ions was assumed in the calculations). We can see a fundamental difference between these two phases. In the former case, the spectrum has a band gap, whereas the band structure in the latter case is of a semimetallic type. With the growing occupancy of the high-spin term occurring on heating, a gradual metallization of the crystal should take place; a more detailed discussion of such behavior is given below. This figure also demonstrates the second feature characteristic of strongly correlated fermion bands; namely, their spectral weight is different at different points of the Brillouin zone; this is indicated by varying thickness of the curves.

In Fig. 3, we show the dependence of the electronic structure of $GdCoO_{3-\delta}$ on temperature and oxygen nonstoichiometry (in experiment, the value of δ is determined by the thermogravimetric analysis and appears to be equal to 0.01). At $T = 0$ and $\delta = 0$,
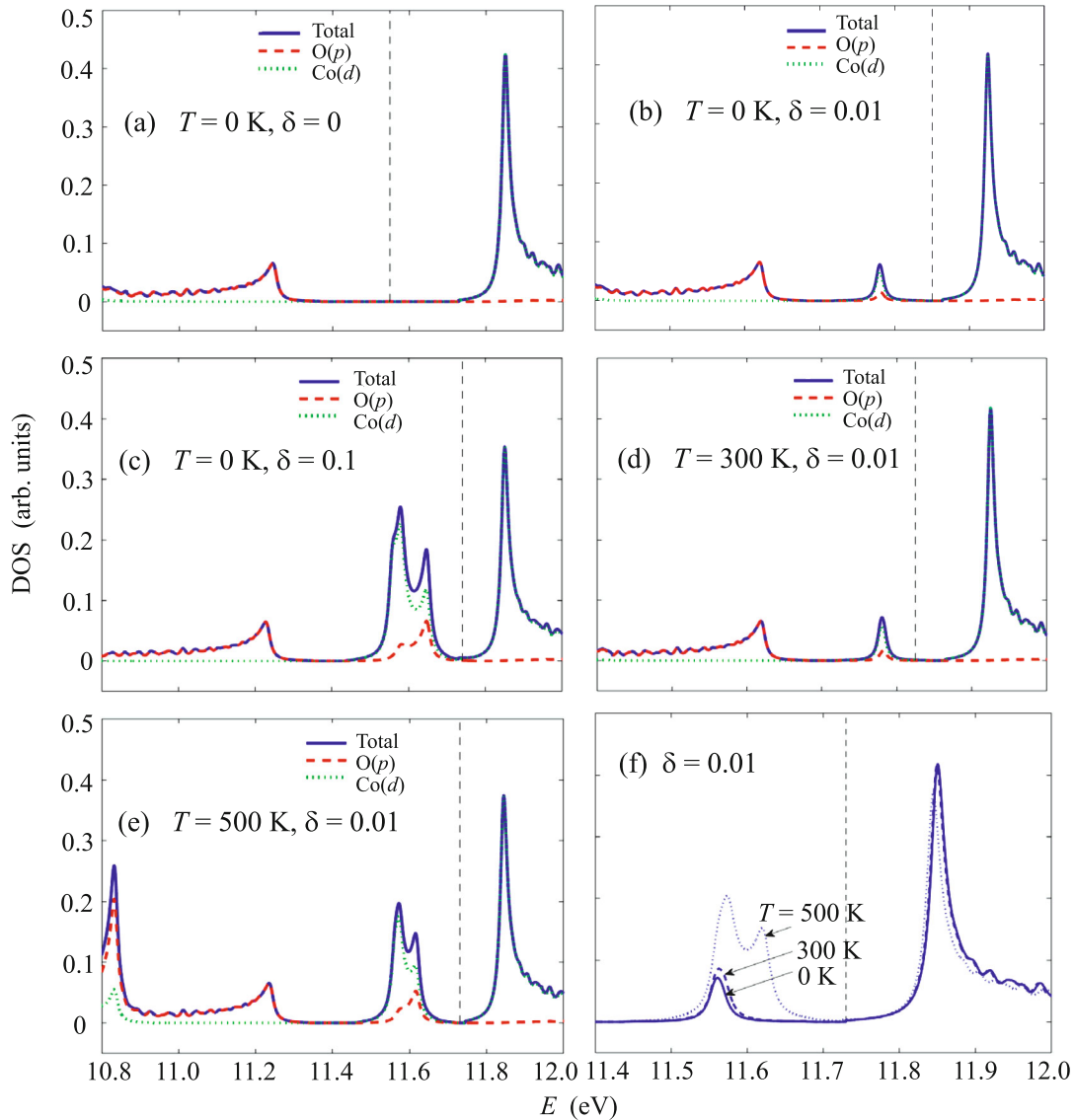
Fig. 3. (Color online) Total and partial densities of states of (a) the GdCoO$_3$ stoichiometric compound at $T = 0$ and (b–e) the GdCoO$_{3-\delta}$ nonstoichiometric compound at $T =$ (b, c) 0, (d) 300, and (e) 500 K calculated using the LDA + GTB method. At $T = 0$ and $\delta = 0$, GdCoO$_3$ is an insulator with the band gap $E_g \approx 0.5$ eV. At $\delta \neq 0$, in-gap states arise below the conduction band and are characterized by the temperature-dependent spectral weight. The dashed line shows the position of the chemical potential. In panel (f) for clearness, we show at a larger scale the plots of the total density of states near the chemical potential at temperatures $T =$ (solid line) 0, (dashed line) 300, and (dotted line) 500 K and at the fixed $\delta = 0.01$.

GdCoO$_3$ is a charge transfer insulator with the band gap $E_g \approx 0.5$ eV (Fig. 3a). With the growth of temperature, the quasiparticle spectrum is determined by the thermally induced occupancy of the HS state of Co^{3+} ions and hence by the spin gap Δ_S. Owing to the temperature dependence of the latter, the band gap E_g in GdCoO$_3$ decreases with the growth of temperature and vanishes at the characteristic insulator–metal transition temperature $T_{\mathrm{IMT}} \approx 780$ K [47]. Note that the transition from the insulating to the metallic state

in rare-earth cobaltites is actually not a phase transition and the band gap is not a thermodynamic order parameter. The quasiparticle band structure at three temperatures $T = 0$, 300, and 500 K and at $\delta = 0.01$ is shown in Figs. 3b, 3d, and 3e, respectively. We can see that some so-called in-gap states appear near the chemical potential within the band gap below the bottom of the conduction band and above the top of the valence band. The temperature-induced increase in the spectral weight and in the band width corresponding to the in-gap states correlates with the observed

shift of the transmittance peak and with the narrowing of the transparency window. For a clearer representation of the data, the plots of the total density of states near the chemical potential at different temperatures $T = 0$, 300, and 500 K (shown by the solid, dashed, and dotted lines, respectively) are presented in Fig. 3f at a larger scale. Note that the electronic structure undergoes similar changes with the growth of temperature at small δ and with the increase in the oxygen nonstoichiometry at low temperatures (Figs. 3c and 3e).

The oxygen nonstoichiometry and thermal fluctuations of multiplicity play an important role in the formation of the electronic structure of cobaltites and of its temperature dependence. In this case, the temperature dependence of the band structure and the existence of in-gap states related to the oxygen nonstoichiometry appear to be principally many-particle effects.

The physical mechanism giving rise to the new states and bands is related to a nonzero contribution to the one-particle density of states coming from the excited multielectron term, which is missing in the case of perfect stoichiometry. It is well known that the impurity levels in usual semiconductors appear owing to fluctuations of the crystal potential occurring near a defect. As we can see, the "impurity-like" levels can appear in the semiconductors with electron correlations, which are discussed here, even in the absence of such fluctuations. We do not take into account any defects in the initially formulated $p-d$ model. In actual materials, the nonstoichiometry surely leads to the fluctuations of the crystal lattice potential and to the quasiparticle scattering by these fluctuations. Therefore, in the calculations related to the specific systems, this new mechanism should be taken into account along with the usual scattering mechanism.

The in-gap states arising even at a low density of oxygen vacancies lead to the narrowing of the transparency window, to the formation of a narrow transmittance peak (an absorption minimum), and to the shift of the optical absorption edge down to 10 meV (see Figs. 3b and 3d) in agreement with experiment (Fig. 1). In Fig. 3, we can also see that the main contribution to the density of states corresponding to the bottom of the conduction band and the band formed by the in-gap states comes from d electrons. At the same time, the electrical conductivity of charge-transfer insulators is mostly due to p electrons of oxygen; therefore, the appearance of in-gap states only slightly affects the electron conductivity. Thus, using the performed calculation and modeling of the electronic structure of the real $GdCoO_3$ crystal inevitably having the deviations from the perfect oxygen stoichiometry, we managed to lift the seeming controversy between the measured electrical transport and optical characteristics.

Similar results were obtained in [56] by studying the effect of nonstoichiometry with the random distribution of vacancies on the electron spectrum of rutile in the framework of the coherent potential approximation. These studies demonstrate that the arising oxygen vacancies lead to the formation of the vacancy peak within the band gap, which is in agreement with the measured photoemission spectra.

4. SPECIFIC FEATURES OF COBALTITES WITH HETEROVALENT SUBSTITUTION

Complex oxides $(A'A'')CoO_{3-\delta}$ (A' is a lanthanide, A'' is an alkaline-earth element, and δ is the parameter characterizing the oxygen nonstoichiometry) with the perovskite structure, where some rare-earth ions are replaced by alkaline-earth ones exhibit an even greater diversity of physical and chemical characteristics [57–63].

A complementary usage of electron, X-ray, and neutron diffraction allows finding out the conditions for the formation of doped single-phase rare-earth cobaltites $Ln_{1-x}Sr_xCoO_{3-\delta}$ ($Ln = La^{3+}-Yb^{3+}$) and reveals a whole set of the tetragonal and orthorhombic superstructures, in which the magnetic and structural characteristics are determined by the type of cations and by the deficit with respect to oxygen (see Fig. 12 in the supplementary material) [64, 65].

The systems with heterovalent substitution exhibit magnetic phase transitions [40], interplay of ferromagnetic and antiferromagnetic exchange interactions, superconductivity [66], colossal magnetoresistance [67], high-temperature ferromagnetism [68], charge ordering [69], electronic phase separation [70, 71], shape-memory effects [72], and the formation of giant polarons at very low concentrations of alkaline-earth elements [73]. All these characteristic features require an adequate theoretical description and experimental verification.

Currently, the most well-studied compositions are the compounds containing lanthanum [57, 62, 74–82] and praseodymium [61, 83–87] replaced by Sr, Ba, or Ca. The number of publications in this field is fairly large, but the nature of the ferromagnetic state in cobaltites with heterovalent substitution is a subject of continuing debate.

The origin of ferromagnetism is traditionally attributed to a change in the charge state of cobalt ions giving rise to the positive exchange interaction between the ions of different valences described in the framework of the double exchange model. The substitution of alkaline-earth ions A'' for some rare-earth ions A'^{3+} leads to the formation of localized holes. In this case, the properties of the $A'_{1-x}Sr_xCoO_{3-\delta}$ system are considered involving the mixing of Co^{3+} and Co^{4+} ionic states. In such a situation, the contribution of Co^{4+} grows gradually with the doping level x [88, 89].
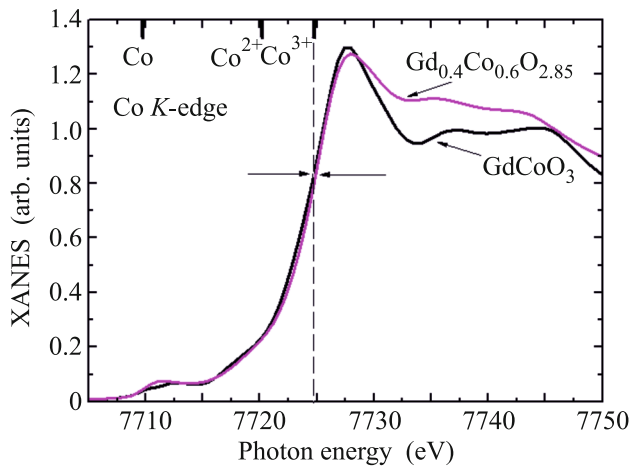
Fig. 4. (Color online) Normalized XANES spectra for the Co K edge measured using the $Gd_{1-x}Sr_xCoO_{3-\delta}$ samples with $x = 0.0$ and 0.6.

Fig. 5. (Color online) XANES spectra for the Gd L_3 edge measured using the $Gd_{1-x}Sr_xCoO_{3-\delta}$ samples with $x = 0.0$ and 0.6 in comparison to those for the reference substance Gd_2O_3.

However, there exist other points of view concerning the valence of Co in these compounds. In [59], it is shown that, in the course of the synthesis of $Sm_{1-x}Ca_xCoO_{3-\delta}$ at normal pressure, the removal of each oxygen ion lowers the local coordination symmetry of transition metal ions from the octahedral to pyramidal one without changing the cobalt valence. Even at low temperatures, Co^{3+} ions in the pyramidal environment turn out to be in the magnetically active state and arranged in a set of pairs formed by individual ions coupled by the antiferromagnetic interaction within the dimer.

We have grown the $Gd_{0.4}Sr_{0.6}CoO_{2.85}$ single crystal by the optical zone melting technique and measured X-ray diffraction and of X-ray absorption spectra (XANES) at the Co K edge (Fig. 4) and at the Gd L_3 edge in $GdCoO_3$ and $Gd_{0.38}Sr_{0.62}CoO_{2.85}$ cobaltites (Fig. 5) and analyzed the effect of Sr substitution on the crystal structure and on the electron and magnetic state of Co ions [90]. It is shown that the strontium doping leads to the enhancement of low-symmetry Jahn–Teller type tetragonal distortions.

As a reference material for determining the charge states of Co ion, we used metallic Co and $Co^{2+}O$ and $Co_2^{3+}O_3$ oxides. In determining the effect of Sr doping on the local structure in the vicinity of Gd, we used Gd_2O_3 oxide as a reference material. The XANES measurements do not reveal any substantial shift of the Co K absorption edge with the increase in the Sr^{2+} content. This could suggest that the effective Co valence (Co^{3+}) does not change, whereas the intensity of the $2p–5d$ dipole transition in the Gd^{3+} ion increases. A probable scenario of the hole doping in
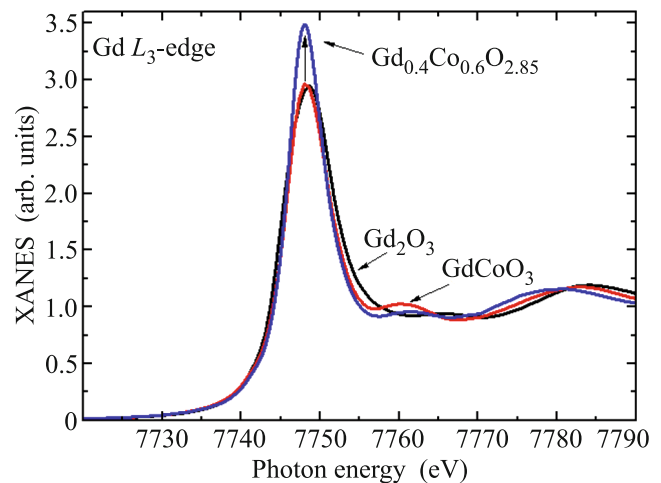
the $Gd_{0.4}Sr_{0.6}CoO_{2.85}$ system is such that holes are partially localized at $2p$ oxygen states and become charge carriers (itinerant holes). In this case, Co($3d$) states and, hence, the effective valence of cobalt should change only slightly. The structural distortions related to the substitution of Sr^{2+} ions for Gd^{3+} ions (namely, the changes in the Gd/Sr–O and Co–O interion distances and of the Co–O–Co bond angle) give rise to the change in the degree of hybridization between the $3d$(Co)–$2p$(O) and $5d$(Gd)–$2p$(O) states and lead to the increase in intensities of the $1s–(p–d)$ (Co^{3+}) and $2p–5d$ (Gd^{3+}) dipole transitions. The holes localized at O($2p$) sites can have a magnetic moment and the interaction of unpaired oxygen spins with the cobalt subsystem can give an additional contribution to magnetism. Appearance of holes at oxygen in the $La_{1-x}Sr_xCoO_{3\pm\delta}$ system has been experimentally confirmed by the XANES and X-ray magnetic circular dichroism (XMCD) measurements at the K edge of oxygen. It is shown that that the growth of x is accompanied by an appreciable growth of the absorption intensity and by the shift of the K edge to the lower energy range (527–529 eV) owing to the increase in the number of unoccupied O($2p$) states [91]. The XMCD intensity increases simultaneously, indicating the nonzero orbital angular momentum of oxygen (appearance of magnetic holes). The magnetic moment at O is directed parallel to that of Co. The problem concerning the nature of hole states in various rare-earth cobaltites requires additional studies, including those implementing the X-ray absorption spectroscopy and XMCD techniques at the oxygen K edge.
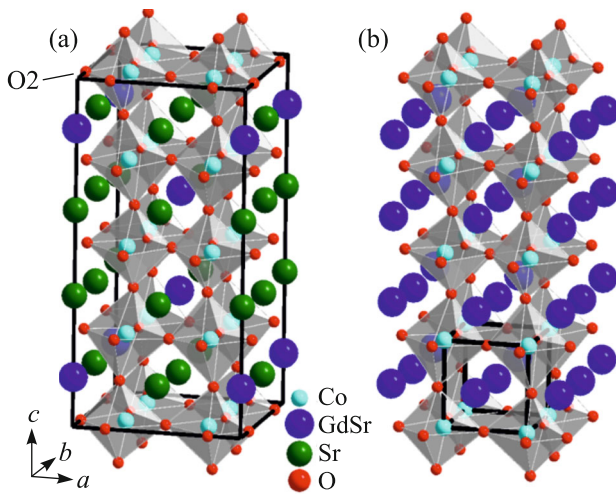
Fig. 6. (Color online) Structure of $Gd_{0.2}Sr_{0.8}CoO_{3-\delta}$ perovskite (a) with the ordered arrangement of cations at A sites and (b) with a disordered occupation of A sites. The black lines indicate the boundaries of a unit cell. Symbol O2 denotes the positions of the preferable location of anion vacancies at room temperature.

Fig. 7. (Color online) Temperature dependence of the linear thermal expansion of $Gd_{0.2}Sr_{0.8}CoO_{3-\delta}$ samples. The inset illustrates the temperature dependence of strain.

The studies of the polycrystalline $Ln_{1-x}M_xCoO_{3-\delta}$ samples demonstrate that the level of oxygen nonstoichiometry appreciably affects the physical and chemical properties of these compounds. The estimation of the oxygen nonstoichiometry is given in many papers [92−94] and the purposeful studies of its effect on the properties of cobaltites are encountered quite often [68, 95, 88, 57, 81]. However, not always does the stabilization of some magnetic state in the cobaltites under study depend only on the degree of oxygen nonstoichiometry. The properties of some compounds are substantially affected by the ordering of cations located at A positions of the crystal lattice. This quite probably leads to the current situation with $Re_{1-x}M_xCoO_{3-\delta}$, for which the results on magnetic susceptibility reported by different authors are not always consistent and reproducible. The possible influence of the characteristics of the A-site cation distribution on the physical and chemical properties is still nearly unexplored [96]. In [97, 98], we have shown that the character of distribution for "inactive" cations over A lattice sites (Fig. 6) significantly affects the properties of $Gd_{1-x}Sr_xCoO_{3-\delta}$ ($0.5 \leq x \leq 0.9$) perovskites, namely, the catalytic activity of the single-phase compounds in the chemical reaction of deep oxidation of methane turns out to be much higher in the case of the disordered (random) distribution of Gd/Sr cations in comparison to that in the sample with the ordered arrangement of Gd^{3+} and Sr^{2+} cations at A sites [97].

In [99], using $Gd_{0.2}Sr_{0.8}CoO_{3-\delta}$ as an example, we have analyzed the experimental data on the magnetic

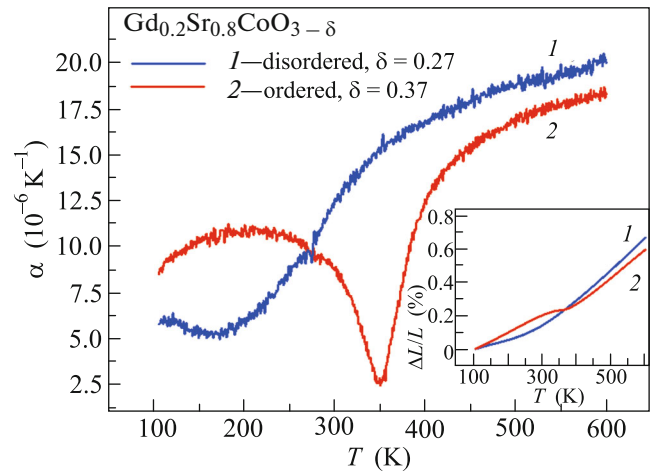susceptibility and thermal characteristics obtained for the compounds with the state (disordered or ordered) specified by the regime of thermal processing and then verified by the precision studies of their crystal structure. In Fig. 7, we demonstrate the considerable difference in the temperature dependence of the thermal expansion coefficients and of the magnetic susceptibility (Figs. 8 and 9) for the ordered and disordered samples, whereas Fig. 10 demonstrates the changes in the behavior of the thermal expansion coefficient related to the higher mobility of oxygen vacancies in disordered samples.
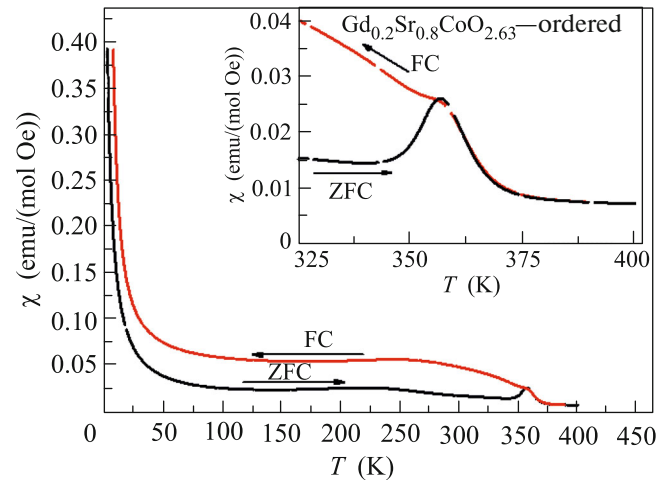

Fig. 8. (Color online) Temperature dependence of the magnetic susceptibility of the ordered $Gd_{0.2}Sr_{0.8}CoO_{3-\delta}$ compound measured in field-cooling (FC) and zero-field-cooling (ZFC) modes at the applied magnetic field $H = 1$ kOe. In the inset, we show for clearness the magnetic susceptibility at temperature ranging from 325 to 400 K.
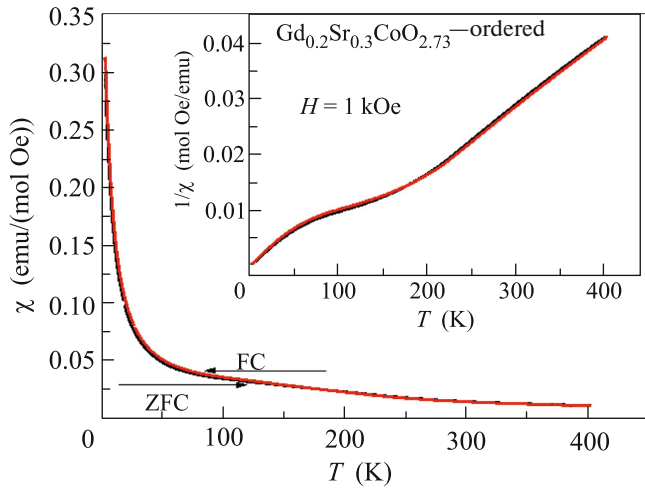
Fig. 9. (Color online) Temperature dependence of the magnetic susceptibility of the disordered $Gd_{0.2}Sr_{0.8}CoO_{3-\delta}$ compound measured in (black curve) FC and (red curve) ZFC modes at the applied magnetic field $H = 1$ kOe. The inset illustrates the temperature dependence of the inverse magnetic susceptibility.

In [100], it is also emphasized that the partial substitution of ions in the A lattice at the same $3d$ cations (at B sites) in $Ln_xM_{1-x}CoO_{3-\delta}$ systems allows us to stabilize the thermally unstable structures.

5. CONCLUSIONS

The rare-earth cobaltites along with cuprates and manganites exhibit some common features characteristic of strongly correlated electron systems. We should mention, first, just the existence of the insulating state in underdoped crystals and, second, a clearly pronounced temperature and doping dependence of the electronic structure, which in the case of cuprates were under discussion for quite a long time [101]. At the same time, they have their own unique features related to the small separation in energy between high- and low-spin terms, which leads to an appreciable contribution of the thermal multiplicity fluctuations to all physical characteristics: electron, magnetic, optical, and structural ones. Just the comprehensive multifaceted studies with the thorough characterization of the samples provide an opportunity of obtaining quite unexpected results, such as the absence of the valence changes of cobalt in $Gd_{0.4}Sr_{0.6}CoO_{2.85}$ single crystals. Such results pose new questions concerning the nature of conductivity and magnetism in doped cobaltites, the studies of which are far from being finished.
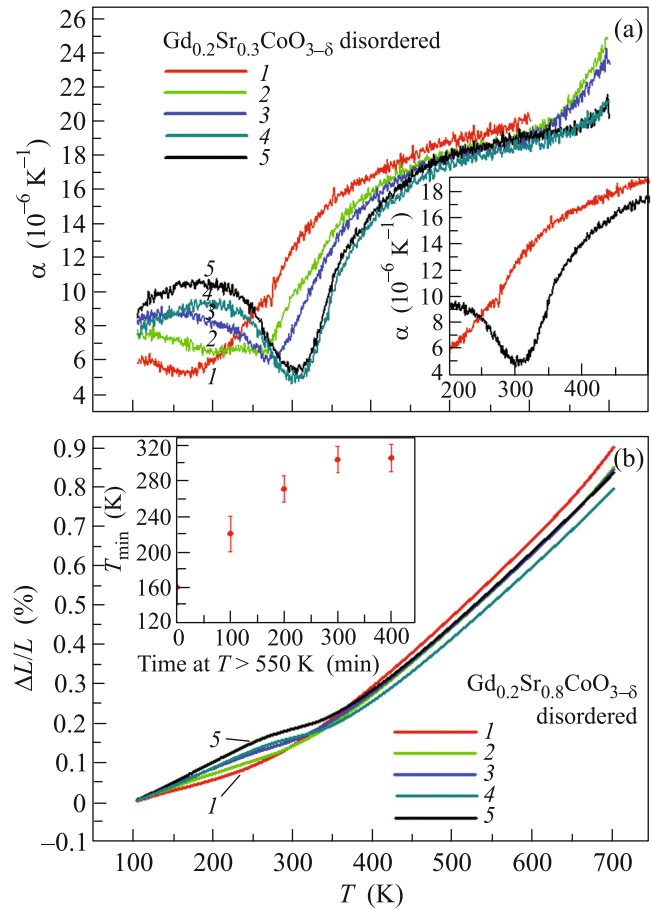
Fig. 10. (Color online) Temperature dependence of (a) the linear thermal expansion α and (b) strain $\Delta L/L$ obtained as a result of the subsequent heating−cooling cycles (from the first to the fifth ones) for the disordered $Gd_{0.2}Sr_{0.8}CoO_{3-\delta}$ compound. In the inset of panel (a), we show for clearness the results for the first and the last cycles. In the inset of panel (b), we show the effect of the time of residence of the sample at a temperature above 550 K on the positions of minima corresponding to the anomaly in $\alpha(T)$.

REFERENCES

1. L. Cambi and A. Cagnasso, Atti Accad. Naz. Lincei, Cl. Sci. Fis., Mat. Nat., Rend. **13**, 809 (1931).

2. Y. Tanabe and S. Sugano, J. Phys. Soc. Jpn. **9**, 753 (1954).

3. H. Spiering, E. Meissner, H. Koppel, E. W. Muller, and P. Gutlich, Chem. Phys. **68**, 65 (1982).

4. I. S. Lyubutin and A. G. Gavrilyuk, Phys. Usp. **52**, 989 (2009).

5. S. G. Ovchinnikov, Yu. S. Orlov, and V. A. Dudnikov, J. Magn. Magn. Mater. **324**, 3584 (2012).

6. T. Vogt, J. A. Hriljac, N. C. Hyatt, and P. Woodward, Phys. Rev. B **67**, 140401 (2003).

7. N. B. Ivanova, S. G. Ovchinnikov, M. M. Korshunov, I. M. Eremin, and N. V. Kazak, Phys. Usp. **52**, 789 (2009).

8. B. Raveau and Md. M. Seikh, *Cobalt Oxides. From Crystal Chemistry to Physics* (Wiley-VCH, Weinheim, Germany, 2012).

9. S. Yamaguchi, Y. Okimoto, H. Taniguchi, and Y. Tokura, Phys. Rev. B **53**, 2926 (1996).

10. V. G. Bhide and S. Rajoria, Phys. Rev. B **6**, 1021 (1972).

11. W. C. Koehler and E. O. Wollan, J. Phys. Chem. Solids **2**, 100 (1957).

12. P. G. Radaelli and S. W. Cheong, Phys. Rev. B **66**, 094408 (2002).

13. J. B. Goodenough, J. Phys. Chem. Solids **6**, 287 (1958).

14. P. M. Raccah and J. B. Goodenough, Phys. Rev. B **155**, 932 (1967).

15. K. Asai, O. Yokokura, N. Nishimori, H. Chou, J. M. Tranquada, G. Shirane, S. Higuchi, Y. Okajima, and K. Kohn, Phys. Rev. B **50**, 3025 (1994).

16. M. A. Senaris-Rodriguez and J. B. Goodenough, J. Solid State Chem. **116**, 224 (1995).

17. R. H. Potze, G. A. Sawatzky, and M. Abbate, Phys. Rev. B **51**, 11501 (1995).

18. T. Saitoh, T. Mizokawa, A. Fujimori, M. Abbate, Y. Takeda, and M. Takano, Phys. Rev. B **55**, 4257 (1997).

19. M. A. Korotin, S. Yu. Ezhov, I. V. Solovyev, V. I. Anisimov, D. I. Khomskii, and G. A. Sawatzky, Phys. Rev. B **54**, 5309 (1996).

20. S. K. Pandey, A. Kumar, S. Patil, V. R. R. Medicherla, R. S. Singh, K. Maiti, D. Prabhakaran, A. T. Boothroyd, and A. V. Pimpale, Phys. Rev. B **77**, 045123 (2008).

21. S. K. Pandey, S. Patil, V. R. R. Medicherla, R. S. Singh, and K. Maiti, Phys. Rev. B **77**, 115137 (2008).

22. S. Noguchi, S. Kawamata, K. Okuda, H. Nojiri, and M. Motokawa, Phys. Rev. B **66**, 094404 (2002).

23. M. W. Haverkort, Z. Hu, J. C. Cezar, T. Burnus, H. Hartmann, M. Reuther, C. Zobel, T. Lorenz, A. Tanaka, N. B. Brookes, H. H. Hsieh, H.-J. Lin, C. T. Chen, and L. H. Tjeng, Phys. Rev. Lett. **97**, 176405 (2006).

24. Z. Ropka and R. J. Radwanski, Physica B **312−313**, 777 (2002).

25. M. Itoh, J. Hashimoto, S. Yamaguchi, and Y. Tokura, Physica B **281−282**, 510 (2000).

26. V. G. Bhide, D. S. Rajoria, and Y. S. Reddy, Phys. Rev. B **28**, 1133 (1972).

27. G. Thornton, F. C. Morrison, S. Partington, B. C. Tofield, and D. E. Williams, J. Phys. C: Solid State Phys. **21**, 2871 (1988).

28. J.-Q. Yan, J.-S. Zhou, and J. B. Goodenough, Phys. Rev. B **69**, 134409 (2004).

29. N. B. Ivanova, N. V. Kazak, C. R. Michel, A. D. Balaev, and S. G. Ovchinnikov, Fiz. Tverd. Tela **49**, 32 (2007).

30. M. J. R. Hoch, S. Nellutla, J. van Tol, E. S. Choi, J. Lu, H. Zheng, and J. F. Mitchell, Phys. Rev. B **79**, 214421 (2009).

31. S. Yamaguchi, Y. Okimoto, and Y. Tokura, Phys. Rev. B **54**, 11022 (1996).

32. K. Knizek, Z. Jirak, J. Hejtmanek, M. Veverka, M. Marysko, G. Maris, and T. T. M. Palstra, Eur. Phys. J. B **47**, 213 (2005).

33. K. Asai, A. Yoneda, O. Yokokura, J. M. Tranquada, G. Shirane, and K. Kohn, J. Phys. Soc. Jpn. **67**, 290 (1998).

34. M. Tachibana, T. Yoshida, H. Kawaji, T. Atake, and E. Takayama-Muromachi, Phys. Rev. B **77**, 094402 (2008).

35. A. Wold and R. Ward, J. Am. Chem. Soc. **76**, 1029 (1954).

36. H. L. Yakel, Acta Crystallogr. **8**, 394 (1955).

37. A. Kappatsch, S. Quezel-Ambrunaz, and J. Sivardiere, J. Phys. France **31**, 369 (1970).

38. G. Thornton, B. C. Tofield, and A. W. Hewat, J. Solid State Chem. **61**, 301 (1986).

39. V. A. Dudnikov, D. A. Velikanov, N. V. Kazak, C. R. Michel, J. Bartolome, A. Arauzo, S. G. Ovchinnikov, and G. S. Patrin, Phys. Solid State **54**, 79 (2012).

40. N. B. Ivanova, N. V. Kazak, C. R. Michel, A. D. Balaev, S. G. Ovchinnikov, A. D. Vasil'ev, N. V. Bulina, and E. B. Panchenko, Phys. Solid State **49**, 1498 (2007).

41. N. B. Ivanova, N. V. Kazak, C. R. Michel, A. D. Balaev, and S. G. Ovchinnikov, Phys. Solid State **49**, 2126 (2007).

42. K. Knizek, P. Novak, and Z. Jirak, Phys. Rev. B **71**, 054420 (2005).

43. M. Itoh, M. Mori, S. Yamaguchi, and Y. Tokura, Physica B **259−261**, 902 (1999).

44. F. G. Birch, Phys. Rev. **71**, 809 (1947).

45. F. G. Birch, J. Geophys. Res. **91**, 4949 (1986).

46. V. A. Dudnikov, S. G. Ovchinnikov, Yu. S. Orlov, N. V. Kazak, K. R. Michel, G. S. Patrin, and G. Yu. Yurkin, J. Exp. Theor. Phys. **114**, 841 (2012).

47. Yu. S. Orlov, L. A. Solovyov, V. A. Dudnikov, et al. (Collab.), Phys. Rev. B **88**, 235105 (2013).

48. S. G. Ovchinnikov, Yu. S. Orlov, V. A. Dudnikov, S. N. Vereschagin, and N. S. Perov, J. Magn. Magn. Mater. **383**, 162 (2015).

49. R. Yu. Babkin, K. V. Lamonova, S. M. Orel, S. G. Ovchinnikov, and Yu. G. Pashkevich, JETP Lett. **99**, 476 (2014).

50. A. Ikeda, T. Nomura, Y. H. Matsuda, A. Matsuo, K. Kindo, and K. Sato, Phys. Rev. B **93**, 220401 (2016).

51. S. G. Ovchinnikov, Yu. S. Orlov, A. A. Kuzubov, V. A. Dudnikov, A. E. Sokolov, V. N. Zabluda, S. B. Naumov, and N. P. Shestakov, JETP Lett. **103**, 161 (2016).

52. V. I. Anisimov, A. I. Poteryaev, M. A. Korotin, A. O. Anokhin, and G. Kotliar, J. Phys.: Condens. Matter **9**, 7359 (1997).

53. S. G. Ovchinnikov, V. A. Gavrichkov, M. M. Korshunov, and E. I. Shneyder, Springer Ser. Solid-State Sci. **171**, 143 (2012).

54. M. M. Korshunov, V. A. Gavrichkov, S. G. Ovchinnikov, I. A. Nekrasov, Z. V. Pchelkina, and V. I. Anisimov, Phys. Rev. B **72**, 165104 (2005).

55. V. A. Gavrichkov, S. G. Ovchinnikov, A. A. Borisov, and E. V. Goryachev, J. Exp. Theor. Phys. **91**, 369 (2000).

56. M. A. Korotin and V. M. Zainullina, Phys. Solid State **55**, 952 (2013).

57. I. O. Troyanchuk, A. N. Chobot, A. V. Nikitin, O. S. Mantytskaya, L. S. Lobanovskii, and V. M. Dobryanskii, Phys. Solid State **57**, 2427 (2015).

58. I. O. Troyanchuk, L. S. Lobanovskii, S. V. Dubkov, Yu. I. Shilyaeva, M. V. Silibin, and S. A. Gavrilov, Phys. Solid State **58**, 293 (2016).

59. T. N. Vasil'chikova, T. G. Kuz'mova, A. A. Kamenev, A. R. Kaul, and A. N. Vasil'ev, JETP Lett. **97**, 34 (2013).

60. A. A. Kozlovskii, V. F. Khirnyi, A. V. Semenov, and V. M. Puzikov, Phys. Solid State **53**, 707 (2011).

61. V. V. Sikolenko, V. V. Efimov, S. Schorr, S. Ritter, and I. O. Troyanchuk, Phys. Solid State **56**, 77 (2014).

62. A. P. Nemudryi, O. N. Koroleva, and Yu. T. Pavlyukhin, Izv. Akad. Nauk, Ser. Fiz. **67**, 951 (2003).

63. N. A. Babushkina, A. N. Taldenkov, S. V. Strelsov, A. V. Kalinov, T. G. Kuzmova, A. A. Kamenev, A. R. Kaul, D. I. Khomskii, and K. I. Kugel, J. Exp. Theor. Phys. **118**, 266 (2014).

64. M. James, L. Morales, and K. Wallwork, Physica B **385−386**, 199 (2006).

65. M. James, T. Tedesco, D. J. Cassidy, and R. L. Withers, Mater. Res. Bull. **40**, 990 (2005).

66. K. Takada, H. Sakurai, E. Takayama-Muromachi, F. Izumi, R. A. Dilanian, and T. Sasaki, Nature **422**, 53 (2003).

67. A. A. Taskin, A. N. Lavrov, and Y. Ando, Phys. Rev. Lett. **90**, 227201 (2003).

68. W. Kobayashi, S. Ishiwata, I. Terasaki, M. Takano, I. Grigoraviciute, H. Yamauchi, and M. Karppinen, Phys. Rev. B **72**, 104408 (2005).

69. Y. Moritomo, M. Takeo, X. J. Liu, T. Akimoto, and A. Nakamura, Phys. Rev. B **58**, 13334 (1998).

70. D. Phelan, D. Louca, S. Rosenkranz, S.-H. Lee, Y. Qiu, P. J. Chupas, R. Osborn, H. Zheng, J. F. Mitchell, J. R. D. Copley, J. L. Sarrao, and Y. Moritomo, Phys. Rev. Lett. **96**, 027201 (2006).

71. J. Wu, H. Zheng, J. F. Mitchell, and C. Leighton, Phys. Rev. B **73**, 020404 (2006).

72. V. P. S. Awana, J. Nakamura, M. Karppinen, H. Yamauchi, and S. K. Malik, J. Magn. Magn. Mater. **250**, 6 (2002).

73. A. Podlesnyak, M. Russina, A. Furrer, A. Alfonsov, E. Vavilova, V. Kataev, B. Buchner, Th. Strassle, E. Pomjakushina, K. Conder, and D. I. Khomskii, Phys. Rev. Lett. **101**, 247603 (2008).

74. I. O. Troyanchuk, D. V. Karpinsky, M. V. Bushinsky, V. Sikolenko, V. Efimov, and A. Cervellino, JETP Lett. **93**, 139 (2011).

75. I. O. Troyanchuk, M. V. Bushinsky, A. V. Nikitin, L. S. Lobanovsky, A. M. Balagurov, V. Sikolenko, V. Efimov, and D. V. Sheptyakov, J. Appl. Phys. **113**, 053909 (2013).

76. J. Mastin, M.-A. Einarsrud, and T. Grande, Chem. Mater. **18**, 1680 (2006).

77. D. Fuchs, M. Merz, P. Nagel, R. Schneider, S. Schuppler, and H. von Lohneysen, Phys. Rev. Lett. **111**, 257203 (2013).

78. R. X. Smith, M. J. R. Hoch, W. G. Moulton, P. L. Kuhns, A. P. Reyes, G. S. Boebinger, H. Zheng, and J. F. Mitchell, Phys. Rev. B **86**, 054428 (2012).

79. R. Lengsdorf, M. Ait-Tahar, S. S. Saxena, M. Ellerby, D. I. Khomskii, H. Micklitz, T. Lorenz, and M. M. Abd-Elmeguid, Phys. Rev. B **69**, 140403(R) (2004).

80. R. Ganguly, M. Hervieu, N. Nguyen, A. Maignan, C. Martin, and B. Raveau, J. Phys.: Condens. Matter **13**, 10911 (2001).

81. J. Pietosa, A. Wisniewski, R. Puzniak, I. Fita, M. Wojcik, W. Paszkowicz, R. Minikayev, J. Nowak, Ch. Lathe, S. Kolesnik, and B. Dabrowski, Phys. Rev. B **79**, 214418 (2009).

82. N. O. Golosova, D. P. Kozlenko, V. I. Voronin, V. P. Glazkov, and B. N. Savenko, Phys. Solid State **48**, 96 (2006).

83. K. Yoshi, M. Mizumaki, Y. Saitoh, and A. Nakamura, J. Solid State Chem. **152**, 577 (2000).

84. K. Yoshii and A. Nakamura, Physica B **281−282**, 514 (2000).

85. I. O. Troyanchuk, D. V. Karpinskii, A. N. Chobot, D. G. Voitsekhovich, and V. M. Dobryanskii, JETP Lett. **84**, 151 (2006).

86. A. M. Balagurov, I. A. Bobrikov, D. V. Karpinskii, I. O. Troyanchuk, V. Yu. Pomyakushin, and D. V. Sheptyakov, JETP Lett. **88**, 531 (2008).

87. A. M. Balagurov, I. A. Bobrikov, V. Yu. Pomyakushin, E. V. Pomyakushina, D. V. Sheptyakov, and I. O. Troyanchuk, JETP Lett. **93**, 263 (2011).

88. R. P. Haggerty and R. Seshadri, J. Phys.: Condens. Matter **16**, 6477 (2004).

89. I. O. Troyanchuk, A. N. Chobot, N. V. Tereshko, D. V. Karpinskii, V. Efimov, V. Sikolenko, and P. Khenri, J. Exp. Theor. Phys. **112**, 837 (2011).

90. M. S. Platunov, V. A. Dudnikov, Yu. S. Orlov, N. V. Kazak, L. A. Solovyev, Ya. V. Zubavichus, A. A. Veligzhanin, P. V. Dorovatovskii, S. N. Vereshchagin, K. A. Shaikhutdinov, and S. G. Ovchinnikov, JETP Lett. **103**, 196 (2016).

91. S. Medling, Y. Lee, H. Zheng, J. F. Mitchell, J. W. Freeland, B. N. Harmon, and F. Bridges, Phys. Rev. Lett. **109**, 157204 (2012).

92. I. O. Troyanchuk, M. V. Bushinsky, V. Sikolenko, V. Efimov, C. Ritter, T. Hansen, and D. M. Tobbens, Eur. Phys. J. B **86**, 435 (2013).

93. D. V. Karpinsky, I. O. Troyanchuk, L. S. Lobanovsky, A. N. Chobot, C. Ritter, V. Efimov, V. Sikolenko, and A. L. Kholkin, J. Phys.: Condens. Matter **25**, 316004 (2013).

94. D. J. Goossens, K. F. Wilson, M. James, A. J. Studer, and X. L. Wang, Phys. Rev. B **69**, 134411 (2004).

95. H. W. Brinks, H. Fjellvag, A. Kjekshus, and B. C. Hauback, J. Solid State Chem. **147**, 464 (1999).

96. M. C. Knapp and P. M. Woodward, J. Solid State Chem. **179**, 1076 (2006).

97. S. N. Vereshchagin, L. A. Solovyov, E. V. Rabchevskii, V. A. Dudnikov, S. G. Ovchinnikov, and A. G. Anshits, Chem. Commun. **50**, 6112 (2014).

98. S. Vereshchagin, L. Solovyev, E. Rabchevskii, V. A. Dudnikov, S. G. Ovchinnikov, and A. Anshits, Kinet. Catal. **56**, 640 (2015).

99. V. A. Dudnikov, Yu. S. Orlov, S. Yu. Gavrilkin, M. V. Gorev, S. N. Vereshchagin, L. A. Solovyov, N. S. Perov, and S. G. Ovchinnikov, J. Phys. Chem. C **120**, 13443 (2016).

100. V. A. Cherepanov, L. Ya. Gavrilova, N. E. Volkova, A. S. Urusov, T. V. Aksenova, and E. Kiselev, Chim. Tech. Acta **2**, 273 (2015).

101. S. G. Ovchinnikov, Phys. Usp. **40**, 993 (1997).

Translated by K. Kugel